Role of Ferroelectricity, Delocalization, and Occupancy of *d* States in the Electrical Control of Interface-Induced Magnetization

Rafael Costa-Amaral[*] and Yoshihiro Gohda[†]

Department of Materials Science and Engineering, Tokyo Institute of Technology, Yokohama 226-8502, Japan

(Received 26 November 2020; revised 30 April 2021; accepted 11 May 2021; published 7 June 2021)

In this study, the influence of generalized-gradient-approximation (GGA) deficiencies, *d*-band occupancy, and itinerancy in the magnetoelectric (ME) effect is investigated from first principles by changing the interface composition of the $Fe_3Si/M/BaTiO_3$ heterostructure, where *M* stands for an atomic layer of pure 3*d* or 4*d* metals (from Sc to Cd). The lattice overestimation of the ferroelectric phase leads to the overestimation of the magnetoelectricity, which can be partially corrected by using the Perdew-Burke-Ernzerhof functional revised for solids. The inclusion of Hubbard-like corrections generally predicts larger changes of interface magnetization upon the reversal of polarization direction, although preserving the trends of plain GGA calculations. The itinerancy of 4*d* states does not favor the interface ME coupling due to the lower density of states near the Fermi level. Here, it is shown how the control of the *d*-state energy levels through their electronic occupancy has the potential to substantially enhance the interface ME effect induced by bonding effects. A substantial increase of magnetoelectricity in the $Fe_3Si/BaTiO_3$ heterostructure can be achieved by replacing interface Fe atoms with V or Mn.

DOI: 10.1103/PhysRevApplied.15.064014

I. INTRODUCTION

The inevitable ending of Moore's law, due to the combination of thermal issues and physical limitations set by the size of the silicon atoms, has led both industry and academia into vigorous research for the substitute of today's silicon-based technology [1]. Although no obvious successor is known, multiferroics hold great promise as their unconventional magnetoelectric (ME) coupling between ferroelectricity and ferromagnetism allows the control of magnetic properties by electric fields, and vice versa. Because the energy required to generate an electric field is substantially lower when compared to its magnetic counterpart, e.g., can be 4 orders of magnitude smaller [2–4], multiferroics could reduce the energy dissipation by Joule heating [5] and push for further miniaturization and energy efficiency in microelectronic devices [4]. Nevertheless, single-phase multiferroics are particularly rare because the transition-metal *d* electrons, which are the usual source of magnetism, prevent the formation of the ferroelectric (FE) soft mode [6]. And when the ferromagnetism and ferroelectricity do coexist, they have limited applicability owing to either a low Curie temperature or a weak coupling.

One way to circumvent this problem is through the combination of a nonferroelectric magnetic material with a nonmagnetic ferroelectric to form the so-called composite multiferroics [4,7]. This approach opens up to the possibility of combining different materials of high Curie temperatures to achieve robust ME coupling at room temperature. In these heterostructures, the ME effect occurs primarily at the interface region and can be induced by distinct mechanisms, such as strain [8–12] or exchange-coupling [13–17]. In carrier-mediated magnetoelectricity [18,19], the ME coupling arises from the capacitive accumulation of spin-polarized carries at the interface as a response to an external electric field. ME effect can also result from bonding effects due to the displacement of the interface atoms caused by the FE instability, changing the overlap between their orbitals [20–22]. In general, interface bonding effects dominate over the screening charge contribution and generate a much stronger coupling when compared to the spin-dependent screening mechanism [23].

As a prototypical room-temperature FE, barium titanate ($BaTiO_3$, BTO) has been widely employed [9,11,21–24] to build lead-free ME composites. BTO has the advantage of being the most consistently researched perovskite material, with very well-documented properties and applications in diversified fields such as data storage [25], nonlinear optics [26], electrochemistry [27]. Among the

[*]amaral.r.aa@m.titech.ac.jp
[†]gohda.y.ab@m.titech.ac.jp

possible ferromagnetic (FM) phases to combine with BTO, the Heusler alloy Fe_3Si emerges as a promising candidate due to its high Curie temperature of 839 K [28] and very low lattice mismatch with BTO. Recently, we study the ME effect at most of the possible interface combinations of the Fe_3Si/BTO heterostructure [22]. We identify that it is very helpful to keep the Si atoms out of the interface, otherwise strong Si—O interactions inhibit the ferroelectric displacement and, consequently, the ME effect. Likewise, the presence of O at the FM side of the interface was found to reduce the ME coupling [21]. Nevertheless, it is possible to stabilize the interface and preserve the ME coupling by inserting a single atomic layer of Co into the Fe_3Si/BTO heterojunction, though the coupling is still weaker than the (unstable) Fe-rich interface.

While a significant share of the microscopic understanding is obtained through generalized gradient approximation (GGA) calculations, GGA functionals present shortcomings that might yield a wrong description of the interfacial magnetoelectricity. For instance, the ferroelectric properties of $BaTiO_3$ are strongly dependent on the volume of the crystal [29], which is known to be, in general, overestimated by GGA functionals such as the Perdew-Burke-Ernzerhof (PBE) version [30]. Furthermore, the underestimation of the band gap due to the self-interaction might lead to an incorrect band alignment and spurious hybridizations at the interface of the heterostructures [31], whereas the more accurate treatment of electronic correlation was found to predict stronger multiferroicity at both $Fe/BaTiO_3$ and $Co/BaTiO_3$ [32].

In this study, we aim to further enhance the ME effect at the interface of the Fe_3Si/BTO by replacing the interface Fe atoms with other 3*d* and 4*d* metals, forming heterostructures designated as $Fe_3Si/M/BaTiO_3$ (M = Sc to Cd). Thus, we can carefully observe the effect of itinerancy and gradual filling of the *d* band on the magnetoelectricity. Density-functional theory (DFT) is used to elucidate the underlying physics at the interface. Concurrently, we address the deficiencies of GGA functionals by employing the PBE revised for solids (PBEsol) [33] together with the Hubbard-U correction [34] to treat the strongly correlated 3*d* electrons. Analysis of interface stability, structural parameters, changes in the interfacial and atomic magnetic moments, charge-density rearrangements, and density of states (DOS) are provided.

We find that the ME coupling is driven by bonding effects at the interface, therefore, it depends on the interface structure, the M—Ti bond length in special, and how much it changes due to the reversal in the polarization direction of the BTO. The stability of the M—Ti bonding results from the interplay between repulsive Coulomb forces and attractive covalent interactions, which contributes to shorten the M—Ti bond when the FE polarization switches from $[00\bar{1}]$ to [001] direction. Because of that, interfaces rich in electropositive metals, such as Sc, Ti, Y, Zr, and Nb, have the atomic positions pinned and the ME effect cannot develop. Likewise, strong depolarization of the FE phase is observed for the late period metals from the Ni, Cu, and Zn groups because their *d* states lie too low in energy to hybridize with the Ti *d* states and stabilize the M—Ti bonding. The depolarization of BTO is weaker for the interfaces rich in V and metals from the Cr, Mn, Fe, Co groups, because the *d* states overlap strongly with the Ti *d* states, which allows the magnetoelectricity to build up. However, the figure of merit is smaller for the corresponding 4*d* metals due to the more itinerant nature of their valence *d* states resulting in lower DOS right above the Fermi level to overlap with Ti *d* states.

We find that the overestimation of the BTO polarization by PBE leads to larger magnetoelectricity when compared to the PBEsol results that predict smaller changes in the interface structure upon the polarization switch. The on-site Coulomb corrections are quantitatively relevant for the interfaces with some multiferroicity, generally increasing the coupling, which is in agreement with previous results [32], but here we validate this trend for a much broader range of systems. The PBEsol + U results indicate that inserting a monolayer of V and Mn to the $Fe_3Si/BaTiO_3$ interface increases the ME effect by up to 12 and 4 times, respectively. For example, the largest calculated ME coefficient estimated for the V-rich interfaces is 8.6×10^{-18} s, which is about 4 times the value found for similar bonding-driven ME heterojunctions [20,21].

II. THEORETICAL APPROACH AND COMPUTATIONAL DETAILS

The first-principles calculations are based on spin-polarized DFT and the Kohn-Sham self-consistent equations are solved using the all-electron projector-augmented-wave [35] (PAW) method as implemented in the Vienna *ab initio* simulation package (VASP), version 5.4.4 [36–38]. Further details on the used PAW projectors are provided in the Supplemental Material [39]. For the exchange-correlation energy functional, the PBE [30] and PBEsol [33] parametrizations are used. Although both functionals are GGAs, the PBEsol is designed to better describe the equilibrium structural properties of bulk solids and surfaces, which helps to address the effects of volume overestimation by PBE on the ME coupling. To treat the strongly correlated valence 3*d* electrons, we use the Hubbard-U correction within the rotationally invariant approach proposed by Dudarev *et al.* [34]. The on-site Coulomb correction is applied to the *d* electrons of the Ti atoms of BTO as well as the M atoms due to the oxidelike environment at the interface of the junction. No corrections are applied to the Fe atoms of the Fe_3Si phase because plain GGA is suitable to describe their metallic behavior. Values of $U_{\text{eff}} = U - J = 4.31$ eV (PBE) and 4.14 eV (PBEsol) are estimated for the Ti sites of

tetragonal BTO through the linear response method [40], as briefly explained in Fig. S1 within the Supplemental Material [39]. On the other hand, we adopt $U_{\text{eff}} = 1$, 2, and 3 eV for the M sites, corresponding to mild-to-moderate level of corrections.

To obtain the equilibrium lattice parameters of the $BaTiO_3$ bulk phase, we use a plane-wave cutoff energy of 830 eV and $8\times8\times8$ **k**-point mesh to integrate the Brillouin zone (BZ). These parameters allow the computation of structural and ferroelectric properties of the tetragonal phase in good agreement with previous calculations [29], as shown in the Supplemental Material [39]. For all the remaining total-energy calculations, we employ a cutoff energy of 466 eV and a $8\times8\times1$ **k**-point mesh to integrate the BZ. A denser mesh of $16\times16\times1$ is used to ensure the convergence of the DOS. For the slab calculations, a vacuum region of 15 Å is adopted. The geometries are relaxed until the atomic forces on every atom are smaller than 0.005 eV $Å^{-1}$, using a total-energy convergence criterion of 10^{-6} eV. These stringent convergence criteria are required for the correct description of the ferroelectric distortions. Three initial magnetic solutions on the M atoms are considered, one ferromagnetic (↑↑) and two antiferromagneticlike: where the M atoms have antiparallel spin with respect to the Fe_3Si (↓↓) and with respect to each other (↑↓). The magnetic solution with the lowest energy is selected for the analysis, details are found in the Supplemental Material [39]. The heterostructures are optimized by the conjugated gradient algorithm with the bottom bilayer being frozen in its bulk position, while the remaining atoms are allowed to relax. Because large values of U_{eff} are reported to kill the ferroelectricity [32], the GGA + U results are obtained by using the respective plain-GGA relaxed structures without further geometric relaxation.

III. RESULTS AND DISCUSSION

A. $Fe_3Si/M/BaTiO_3(001)$ heterostructures

Fe_3Si is a binary $D0_3$-type Heusler alloy with face-centered cubic structure ($Fm\bar{3}m$) and ferromagnetic properties. In this study, $BaTiO_3$ is assumed to be in the tetragonal structure ($P4mm$), which is stable at room temperature. In this phase, the ferroelectricity arises mainly from the relative displacement along the [001] direction of titanium from its centrosymmetric position in the unit cell. The PBE optimization of bulk volume yields lattice parameters $a = b = 4.00$ Å and $c = 4.23$ Å in good agreement with previous results for $BaTiO_3$ [29]. The nearly perfect matching of tetragonal $BaTiO_3$ and Fe_3Si lattices [Fig. 1(a)], where the experimental and computed mismatches are 0.08 and 0.97%, respectively, makes the

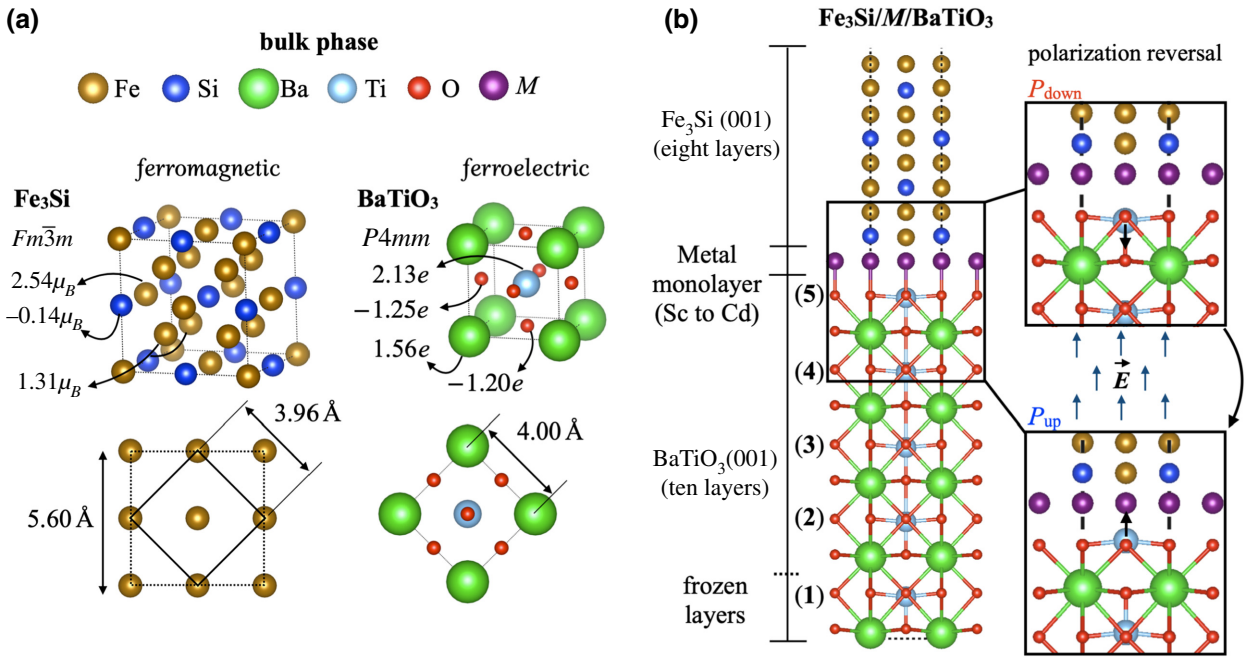

FIG. 1. (a) Bulk structures of Fe_3Si ($Fm\bar{3}m$) and $BaTiO_3$ ($P4mm$). The PBE local magnetic moment for each atomic site is shown for Fe_3Si, whereas the effective Bader charges are presented for $BaTiO_3$. The top view with the in-plane lattice parameters obtained from PBE is shown, which correspond to a lattice mismatch of 0.97%. (b) The side view of the $Fe_3Si/M/BaTiO_3(001)$ heterostructures having the TiO_2 termination. The ferroelectric polarization reversal in the [001] direction is depicted.

$Fe_3Si/BaTiO_3(001)$ interface a promising model for computational studies of ME coupling. Nevertheless, PBE predicts larger values of the c/a ratio and macroscopic polarization when compared to the experiments [41,42] due to the overestimation of the crystal volume [29]. From the results presented in Table S2 within the Supplemental Material [39], PBEsol yields smaller lattice parameters as expected, namely, $a = b = 3.97$ Å and $c = 4.07$ Å, reducing the errors relative to the experiments for c/a and macroscopic polarization from 4.8 to 1.64% and from 75.4 to 30.0%, respectively. As shown, these results have profound implications on the magnetoelectricity.

A continuous superlattice is commonly used to concurrently simulate more than one interface in FM-FE heterostructures [20,21,43]. However, this approach does not take into account surface effects, which may promote changes in the interlayer spacing or surface reconstructions that will necessarily affect ferroelectric properties [44,45]. Therefore, we use the repeated slab geometry, which allows us to include surface effects at the cost of evaluating one interface per calculation.

Because we consider the BTO as a substrate for the Fe_3Si film, the surface-cell in-plane lattice constant is constrained to the computed value of BTO. To check the possible implications of the lattice constraint on the magnetic phase, we calculate the bulk properties of Fe_3Si using the BTO constrained and its equilibrium lattice parameters. As shown in the Supplemental Material [39], the unconstrained results are in line with previous computational [46] and experimental results [47–49]. As expected, the BTO-constrained results indicate that the small lattice mismatch exerts negligible changes on the charge distribution and magnetic properties of Fe_3Si. The heterostructures are formed by stacking nine layers of $Fe_3Si(001)$ on ten layers of $BaTiO_3(001)$, which ensure that the inner layers have a bulklike environment. The interfacial layer of the magnetic phase is replaced by a monolayer of 3*d* or 4*d* metals (from Sc to Cd) to form the $Fe_3Si/M/BaTiO_3$ heterostructures. Here, we consider the TiO_2-terminated interface with the M atoms located on top of the O atoms because it is the most stable configuration for M/BTO interfaces, as previously shown for $Co/SrTiO_3$ [50], $Fe/BaTiO_3$ [20], and $Fe_3Si/BaTiO_3$ [22]. Hence, our systems are set up as $(Fe_2\text{-}FeSi)_4\text{-}M_2\text{-}TiO_2\text{-}(BaO\text{-}TiO_2)_4\text{-}BaO$. To mimic the electric polarization reversal due to the influence of an applied electric field, we built two configurations for each $Fe_3Si/M/BaTiO_3$ system, namely, with BTO ferroelectric distortion in the [001] (P_{up}) and [00$\bar{1}$] (P_{down}) directions, as shown in Fig. 1(b).

B. Interfacial stability

Aside from the lattice mismatch, the magnitude of the interaction between Fe_3Si/M and BTO can be used to evaluate the stability of the interface and to anticipate how effective it would be to epitaxially grow the magnetic phase on $BaTiO_3$ films. To quantify the binding between the two phases, we calculate the interfacial separation work, W_{sep}, defined as

$$W_{sep} = (E^{Fe_3Si/M} + E^{BaTiO_3} - E^{Fe_3Si/M/BaTiO_3})/A, \quad (1)$$

where $E^{Fe_3Si/M}$ and E^{BaTiO_3} are, respectively, the total energies of the isolated Fe_3Si/M and $BaTiO_3$ slabs in their relaxed geometries. $E^{Fe_3Si/M/BaTiO_3}$ is the total energy of the heterostructure, and A is the interfacial area. The results are shown in Fig. 2 (PBEsol) and Fig. S3 (PBE) within the Supplemental Material [39].

Among the systems, W_{sep} varies from 0.05 up to 0.25 eV $Å^{-2}$ and presents a volcano-shaped curve along the period, which peaks at V and Mo for the 3*d* and 4*d* metal monolayer, respectively. The largest values are found for the early transition metals (TM), from the Ti, V, and Cr groups, and decreases with the filling of the *d* band, especially for the 4*d* metals, reaching the lowest values for the metals from Cu and Zn groups. Despite being in a different coordination regime, these results correlate well with the binding strength of metal adatoms on MoS_2 [51,52], graphene [53], and $BaTiO_3(001)$ surfaces [54], e.g., the M/substrate interfaces with larger separation work are associated with larger binding energies of M adatoms on the respective substrate. The W_{sep} trends can be partially explained by the nature of the M—O interfacial bonding, which is more ionic (and stronger) for the early TMs due to their smaller electronegativity [54]. However, because the M monolayers are constrained to the BTO lattice constant, metals with larger atomic radii [55] than Fe (1.40 Å) should experience a compressive strain that destabilizes the interface. This would explain why Sc (1.60 Å), Y (1.80 Å), and Zr (1.55 Å) form less stable interfaces than V (1.35 Å) despite having lower electronegativities. The P_{down} polarization (data in red) slightly favors the interaction because the FE displacement naturally pushes the interfacial O towards the M monolayer, which enhances the M—O bonding. Nevertheless, the reversal of the polarization causes differences in the interfacial separation work of about $1 \sim 10$ meV $Å^{-2}$ [Table S5 (PBEsol) within the Supplemental Material [39]]. These values are compared with those presented by van der Waals (vdW) bonded heterostructures like CrI_3/Sc_2CO_2 (4 meV $Å^{-2}$) [56], which stems from the bistable nature of the $Fe_3Si/M/BaTiO_3$ FE switch. The PBE results present the same trends but predict larger bond lengths and smaller values of W_{sep}, i.e., slightly weaker interaction, which is ultimately a consequence of PBE violating the gradient expansion of the exchange energy functional for slowly varying densities [33].

C. Interfacial magnetization change

Potential candidates for multiferroic based devices should have their magnetic properties changed accordingly

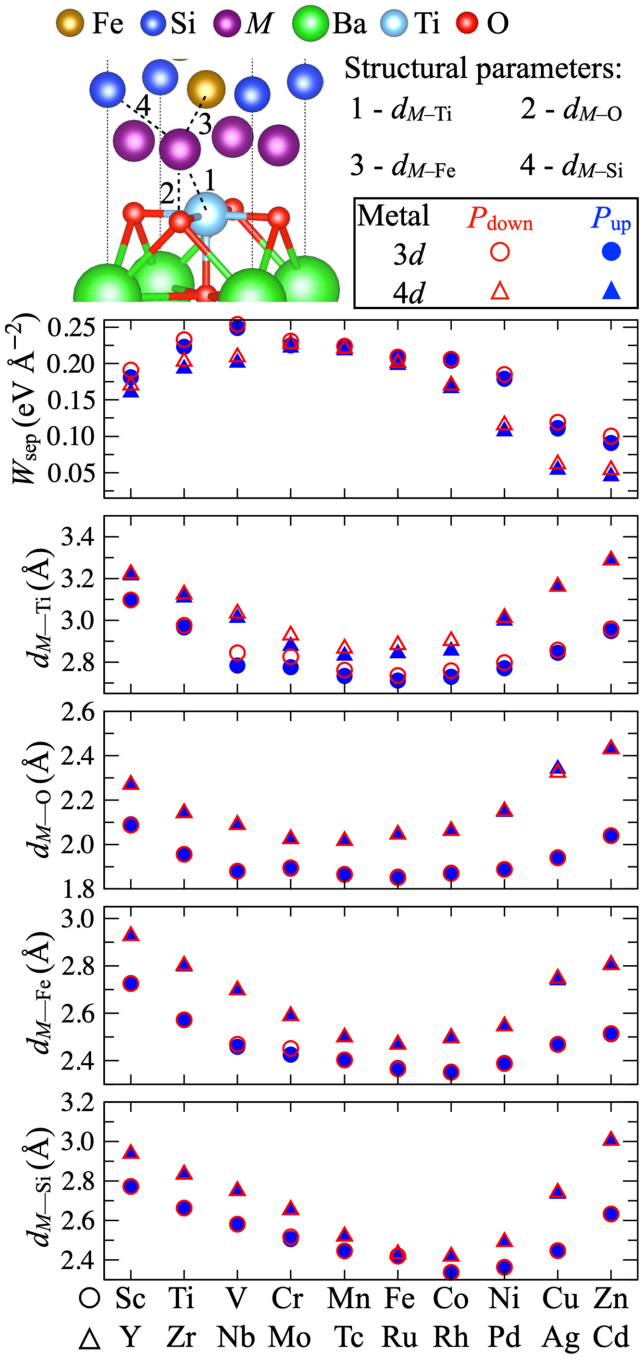

FIG. 2. PBEsol results for the interfacial separation work, W_{sep}, and structural parameters used to characterize the interfacial region of the $Fe_3Si/M/BaTiO_3$ heterostructures. The shortest distance between M and Ti, O, Fe, and Si atoms, d_{M-Ti}, d_{M-O}, d_{M-Fe}, and d_{M-Si}, respectively.

by the effect of an applied electric field. In our systems, we search for possible changes on the magnetic properties of the magnetic phase, Fe_3Si/M, caused by the interchange of $BaTiO_3$ between two distinct FE arrangements, namely, P_{up} and P_{down} [Fig. 1(b)]. This switch could be achieved by, for example, the incidence of an electric field perpendicular to the interfacial plane. To evaluate the ME coupling, we calculate the magnitude of the change in the interfacial magnetic moment, Δm_{int}, upon the polarization reversal of the FE phase. Δm_{int} takes into account the changes in the local magnetic moments of the interfacial atoms (M, Ti, and O), which are obtained by the integration of the spin-polarized charge density enclosed within the Bader volumes [57]. The same method [57] is employed for the effective charge analysis in this study. The results are shown in Fig. 3.

Overall, larger changes of interfacial magnetic moment, Δm_{int}, are found for the interfaces rich in metals from the middle of the d-block elements except for Cr. For instance, upon the switch of the polarization direction, PBE predicts changes of 0.37, 0.06, 1.04, and 0.46μ_B for M = V, Cr, Mn, and Fe, respectively. We also observe that the ME effect is much weaker for the interfaces with 4d metals, in part due to the diffuseness of the 4d states, as we discuss in Sec. G. PBEsol presents similar trends but predicts much smaller changes of interface magnetization and this is rather caused by differences in interface geometry due to the partial correction of BTO overpolarization than by the differences between the GGA formulations. For example, the magnetization change found for $Fe_3Si/Fe/BaTiO_3$ is about 50% larger than the one reported for $Fe/BaTiO_3$ [20] (0.3μ_B) despite the similarities in the interfacial composition and both being obtained from PBE calculations ran in the same code. The main difference resides in the BTO lattice parameter, the authors used the experimental value, which possibly decreased the overpolarization of BTO.

In agreement with previous results [32], the addition of the on-site U correction to the 3d metals generally increases the magnetization change and is more relevant to the systems, which already present significant ME coupling, specially at the V- and Mn-rich interfaces, which present the largest magnetization changes. The results for the Mo-rich interface also indicate that an enhancement of the ME coupling should be expected for 4d metals as well. In most of the cases, the enhancement of the magnetoelectricity follows the increase of the U_{eff}, exceptions are found among the PBE + U results, demonstrating that the coupling is very responsive to the applied correction. To understand the trends of Δm_{int} and elucidate the origin of the large ME effect found at the V- and Mn-rich interfaces, we perform an in-depth examination of the structural and electronic properties of the $Fe_3Si/M/BaTiO_3$ systems, results of which are presented and discussed in the following sections.

D. Ferroelectric polarization and structural properties

The coupling of magnetic and ferroelectric orders in FM-FE heterojunctions implies in an intrinsic dependence of the magnetization changes on the atomic arrangements,

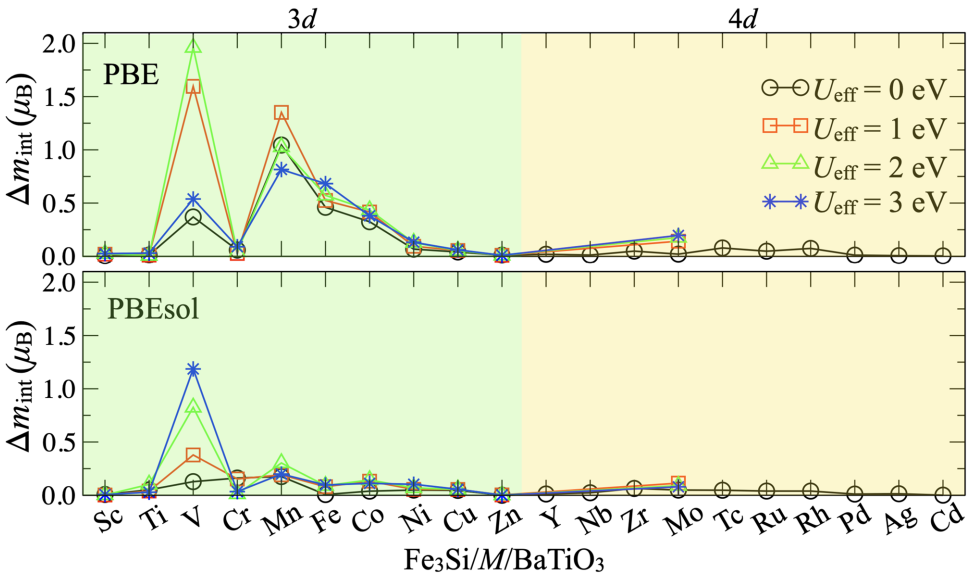

FIG. 3. The amplitude of the interfacial magnetic moment change, Δm_{int}, upon the polarization reversal in the $Fe_3Si/M/BaTiO_3$ heterostructures. For the GGA + U calculations, the Hubbard-U corrections at the Ti sites of BTO are 4.31 eV (PBE) and 4.14 eV (PBEsol).

especially, at the interfacial region. Initially, we analyze the interface atomic setting, characterized by the minimal bonding distances between the M atoms and the remaining nearby species, namely, d_{M-Ti}, d_{M-O}, d_{M-Fe}, and d_{M-Si}, which are shown in Fig. 2 and Fig. S3 within the Supplemental Material [39]. For our systems, two main trends are identified. For metals within the same group, the 4d metals form longer bond lengths with the surrounding atoms mainly due to their larger atomic radius. The general decrease of the atomic radius along the period could explain the initial decrease of the bond lengths from Sc to Cr group, whereas the weakening in interfacial bonding (see W_{sep}) would justify the increase in bond lengths observed from Co to Zn groups. Between the Cr and Co groups, size and bonding effects compete to result in a bowl-shaped curve, especially for the d_{M-Ti} and d_{M-O} parameters. By switching the polarization from P_{down} to P_{up}, we observe an expected decrease in the d_{M-Ti} bond length of about 0.01 $\sim$ 0.15 Å (PBE), with the largest values being associated with the largest ME effects. PBEsol predicts much smaller changes in d_{M-Ti}, namely, from negligible values up to 0.06 Å, which can explain the decrease in the ME effect shown in Fig. 3. No significant changes are found for the other parameters, except for a slight shortening of d_{M-Fe} for V, Cr, and Mn in the PBE results, suggesting that the P_{up} polarization strengthen the M—Fe interactions.

The absence of large bond changes for most of the studied systems may indicate the pinning of interface atomic positions and the occurrence of depolarization effects in the FE phase. To assess the polarization along the stacking direction of BTO, we calculate the rumpling parameter for each TiO_2 layer, defined as the relative displacement between the Ti and O ions. The results for the heterojunctions and bare BTO films (for reference), in both P_{up} and P_{down} configurations, are displayed in Fig. 4 and Fig. S4 within the Supplemental Material [39]. The degradation of the ferroelectric polarization of $BaTiO_3$ is well known in particulate [44] and thin-film geometries [45]. It can be observed for the results of bare BTO surfaces (dotted lines), which have their polarization suppressed by depolarization fields due to the accumulation of charges at the surface [58]. With the formation of the $Fe_3Si/M/BaTiO_3$ interfaces, one would expect M free charges to partially compensate the BTO surface polarization charges and, thus, mitigate the depolarization. However, for most systems in the P_{up} configuration, we observe the opposite behavior, i.e., a much stronger depolarization takes place when compared to the clean surfaces. Note that, for the systems where it occurs, negligible ME effect is observed because the atomic environment at the interface remains virtually unchanged, as shown for the bonding parameters in Fig. 2. A similar behavior is found at the Si-terminated interface of Fe_3Si/BTO because the strong Si–O interactions prevent the change of the ferroelectric displacement upon polarization reversal [22]. The depolarization is much weaker in the PBE results because of the overestimation of FE displacements, which leads to larger interface atomic changes upon polarization reversal and, consequently, the pronounced ME coupling.

The depolarization of the heterojunctions results from the interplay of several factors and can be rationalized in terms of the properties of the M components as follows. At the interfaces where M = Sc, Ti, Y, Zr, or Nb, the depolarization is enhanced by their larger cationic charge, which reduces the screening ability of the M atoms. Furthermore, strong Coulomb interactions increase the attraction of O anions toward the interface while the Ti cations are repelled by the M cations due to strong repulsive electrostatic forces, especially critical for the P_{up} structures.

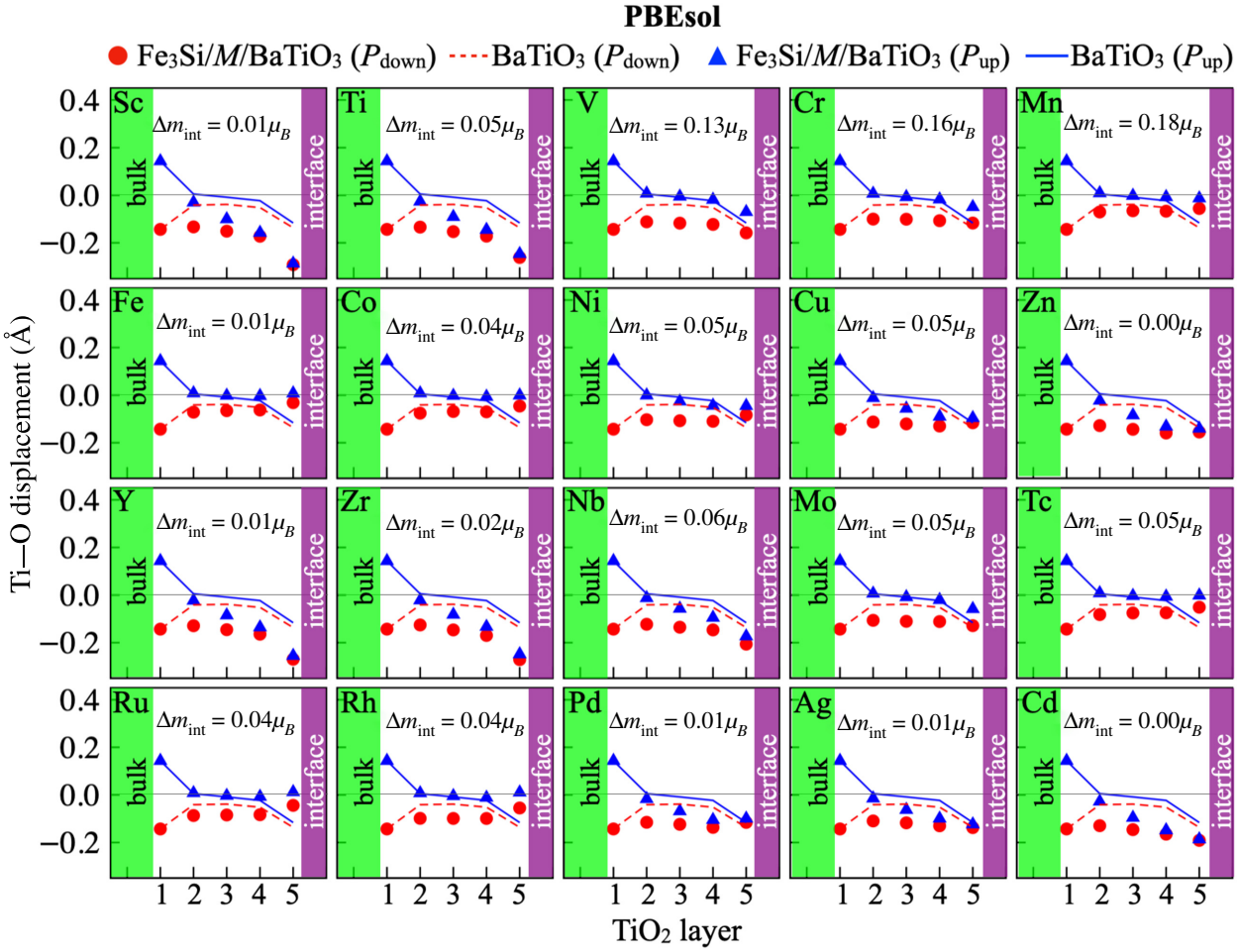

FIG. 4. The PBEsol relative Ti—O displacement along the $BaTiO_3$ film for the $Fe_3Si/M/BaTiO_3$ heterostructures in both P_{up} and P_{down} configurations [as illustrated in Fig. 1 (b)]. The dashed red and solid blue lines represent the values for the clean surface of $BaTiO_3$. The respective interfacial magnetic moment change, Δm_{int}, is given for each system.

A correlating finding was reported for the $Fe_3O_4/BaTiO_3$ interface [21], where a strong interfacial bonding was responsible for pinning the positions of the interface atoms, inhibiting the FE displacement. When M is Ni, Cu, Zn, Pd, Ag, or Cd, the P_{up} is suppressed as well but to a lesser extent because the M monolayers exhibit more charge neutrality. However, most of these interfaces present the lowest values of W_{sep} (see Fig. 2), i.e., have a weaker interfacial bonding due to the filled d-band states, which hinders the formation of the soft mode in the tetragonal BTO film. The depolarization of BTO is lessened for the interfaces composed by V, and metals from the Cr, Mn, Fe, and Co groups, which, based on the discussion so far, should present the right balance between ionic and covalent interactions so that the M—Ti hybridization overcomes the M—Ti repulsion. Although the FE distortion being a *conditio sine qua non* for the occurrence of the ME effect in present junctions, the variety of Δm_{int} among these systems indicates that other variables should play a role in the large ME coupling found for V and Mn systems.

E. Atomic effective charges and interfacial charge transfer

Charge-transfer effects are reported to significantly change the magnetic moment of atoms at the interface of metal-oxide junctions [43], and can provide information to understand the ME coupling in the present systems. First, we calculate the effective charges of each atomic species X, Q^X_{eff}, which is defined as $Q^X_{eff} = Z_{val} - Q^X_{Bader}$, where Z_{val} is the number of valence electrons and Q^X_{Bader} the Bader charge [57]. The charge transfer between the Fe_3Si/M and BTO upon the interface formation, ΔQ_{int}, is given by the sum of the Q^X_{eff} for all the atoms of the magnetic phase, the results are summarized in Table S6 within the Supplemental Material [39]. Our results indicate that the charge flows from Fe_3Si/M to BTO by amounts ranging from 0.12 to 0.80 e (PBE) and from 0.13 to 0.77 e (PBEsol). From a purely electrostatic model [59,60], the Fermi level of a metal-semiconductor junction should be positioned within the band gap of the semiconductor to achieve the charge neutrality and avoid an unrealistic polarization of

the metal and semiconductor bulk states [43,61,62]. Hence, the charge exchanged between the two phases creates an interface dipole to compensate the difference in work function and Fermi level between the magnetic phase and BTO [63], and the larger the Fermi-level mismatch, the larger should be the dipole to balance the charges within the interface. However, the charge transfer is ultimately caused by the polarized M—O bonds at the junction interface, and as such depends on the composition and structure of the interface [60].

Previous studies on Schottky barrier heights have shown that the electronegativity is the most relevant property to control the overall interface dipole and, consequently, the charge transfer among the interface atomic species [64,65].

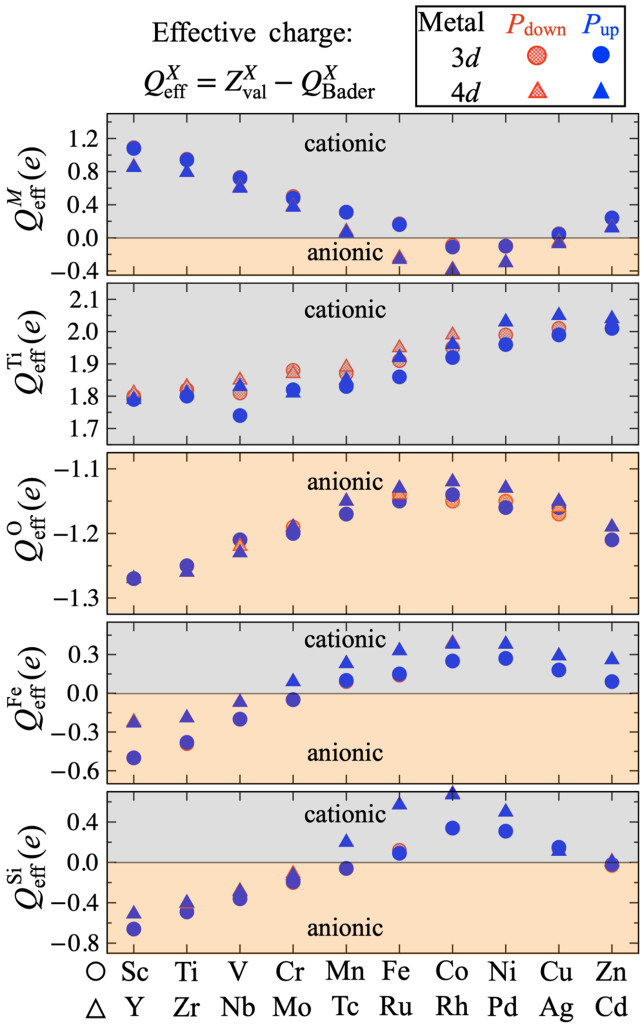

FIG. 5. The PBEsol-averaged effective charges by species, $Q^X_{\rm eff}$, for the interfacial atoms M, Ti, and O, and includes the nearest neighbors Fe and Si atoms. Gray and orange regions indicate if the species are in a cationic or anionic state. Here, $Z^X_{\rm val}$ and $Q^X_{\rm Bader}$ represent the number of valence electrons and the Bader charge, respectively.

As displayed in Fig. 5 and Fig. S5 within the Supplemental Material [39], the atomic charge of M atoms changes significantly among the considered species, e.g., from around -0.39 (Rh) up to 1.08 e (Sc). The gradual decrease of M cationic character correlates with the electronegativity increase along the period, as observed by adsorption studies of 3d and 4d metals on BTO [54] and different substrates [51–53]. Likewise, the electronegativity trend helps to explain the amount of charge flow shown in Table S6 within the Supplemental Material [39] as follows. Replacing surface Fe atoms of the isolated Fe_3Si by more electronegative metals creates an out-of-surface dipole that decreases the Fermi level of the Fe_3Si and the Fermi-level mismatch with $BaTiO_3$. Consequently, less charge is transferred as observed for Ni, Ru, etc., whereas the opposite occurs for less electronegative M like Sc, Y, or Ti. Notice that the effective charges for the interfacial Ti, O, Fe, and Si are also governed by the electronegativity difference of M and the respective species. Therefore, Si ($\chi = 1.90$) can be anionic, when bonded with V ($\chi = 1.63$), or cationic, when bonded with Pd ($\chi = 2.20$).

A change in the effective charges should be expected due to differences in the interface structure promoted by the FE polarization reversal. Our results indicate that only the interface Ti and O atoms present significant changes in the effective charge. For instance, the BTO switching from $P_{\rm down}$ to $P_{\rm up}$ reduces the positive charge of interfacial Ti ions by up to 0.16 e (PBE) and 0.07 e (PBEsol). As shown in Fig. S6 within the Supplemental Material [39], this reduction correlates with the decrease of M—Ti bond lengths and, thus, with the stretching of the Ti—O bond perpendicular to the interface, which is known to cause substantial changes on the atomic charge balance [66]. Nevertheless, the magnitude of charge flow induced by the polarization reversal is much smaller than the observed changes in the local magnetic moments of the respective atoms, suggesting that the magnetoelectricity of the present systems is primarily driven by a different mechanism (e.g., chemical bonding) other than charge transfer.

F. Local magnetic moments

To find the source of the ME effect, we first identify the contribution of each atom to the interfacial magnetic moment change, $\Delta m_{\rm int}$, by looking at how their local magnetic moments vary upon the reversal of the FE polarization. Here we discuss the results for the V-, Cr-, Mn-, and Fe-rich (default $Fe_3Si/BaTiO_3$) interfaces, where the PBEsol + U results of averaged local magnetic moments and changes for the interfacial M, Ti, and O atoms are summarized in Table I. The complete set for all the systems, including data for plain GGA and the near-interface Fe and Si atoms is presented in Table S8 within the Supplemental Material [39].

TABLE I. The PBEsol + U ($U_{\text{eff}} = 3$ eV) averaged local magnetic moments, m_{loc} (in μ_{B}), of the interfacial atoms by species, namely, M, Ti, O, for the V-, Cr-, Mn-, and Fe-rich interfaces in both P_{down} and P_{up} configurations. The change in the m_{loc} for the respective species, Δm_{loc}, upon the switch from down to up polarization.

	$m_{\text{loc}}^{\text{down}}$			$m_{\text{loc}}^{\text{up}}$			Δm_{loc}(up − down)		
System	M	Ti	O	M	Ti	O	M	Ti	O
V	0.09	0.22	0.01	−0.49	0.22	0.04	−0.58	0.01	−0.02
Cr	3.27 (−3.32)	−0.04	−0.04	3.23 (−3.24)	−0.05	0.05	−0.04 (0.08)	−0.01	0.00
Mn	−3.51	0.36	−0.04	−3.43	0.48	0.05	0.09	0.12	−0.01
Fe	2.65	−0.40	0.06	2.65	−0.50	0.06	0.01	−0.11	0.00

For the Fe-rich junction in P_{down} polarization, the magnetic moment of interface O ions is $0.06\mu_B$, whereas the induced magnetic moment of Ti ($m_{\text{loc}} = 0.40\mu_B$) is aligned antiparallel to the Fe magnetic moment. This same magnetic arrangement is found for the Fe/BTO [20] interface, which has a similar interface composition, with differences in the magnitude of the magnetic moments due to the moderate level of U correction. Both Cr- and Mn-rich interfaces present ferrimagnetic solutions with respect to itself and to the Fe atoms of the magnetic phase, e.g., the local magnetic moments in the P_{down} configuration are $3.27(-3.32)\mu_B$ and $-3.51\mu_B$, respectively. We notice that the GGA calculations without U correction predict larger polarization-induced changes of magnetization at the M sites of both systems, indicating a strong ME coupling. However, because the Cr atoms have antiparallel spins with respect to each other, the changes of m_{loc} in each site have opposite signs, which results in a small net change of interface magnetization. Therefore, our results indicate that interface atoms of the magnetic phase in multiferroic heterojunctions should have a parallel arrangement of spins for better efficiency in applications that requires large changes of magnetization controlled by electric fields. The magnetic moment of the V atoms are comparatively smaller and presents parallel or antiparallel configuration with respect to the Fe_3Si depending on the value of the on-site correction. For example, upon the P_{down} to P_{up} switch, the local magnetic moment of V flips from 0.09 to $-0.49\mu_B$, which indicates that most of the ME effect at the Fe_3Si/V/BTO interface comes from each M site. This is different from what is reported for other heterostructures, as Fe/BTO [20], $Fe_3O_4/BaTiO_3$ [21], and Fe_3Si/Co/BTO [22], where most of the magnetization change is due to the interface Ti atoms.

G. Interfacial electron density and density of states

The bonding-driven nature of the ME effect in our systems can be confirmed from the analysis of electron density rearrangements upon the formation of the interface and from the local density of states (LDOS) for the interface atoms. For the sake of conciseness, we show the results for the V-rich interface only, since the results presented in the Supplemental Material [39] points to a similar mechanism for the remaining heterostructures. Figure 6(a) shows the contour of the electron density difference, $\Delta\rho$, for the V-rich interface, defined as $\Delta\rho(\mathbf{r}) = \rho^{Fe_3Si/M/BTO}(\mathbf{r}) - \rho^{Fe_3Si/M}(\mathbf{r}) - \rho^{BTO}(\mathbf{r})$. When the interface is formed, we notice an augmentation of electron density around the interface Ti and O atoms, which is in agreement with our Bader analysis indicating that charge is transferred from the FM to the FE phase. The increase of charge density in the interface region due to the formation of V—O and V—Ti bonds is also associated with the formation of an interface dipole to ensure the charge neutrality [43,61,62]. These features are enhanced when the FE phase reverses its polarization towards the interface, which promotes the Cr—Ti bonding. The interface formation also increases the electron density in the interlayer region of the FM phase as indicated by the population of d_{xz}- and d_{yz}-shaped regions around the Fe atoms, which correlates with the magnetic changes of deeper layers.

Figure 6(b) shows the orbital-resolved LDOS for the interface V and Ti atoms in both polarizations of the V-rich interface. The complete set of LDOS for V, Cr, Mn, Fe, and Mo is shown in the Supplemental Material [39]. As observed by Duan *et al.* [20], the induced magnetization on Ti can be explained by the hybridization of Ti d_{xz} states with the exchange-split d_{xz} states of V, producing exchange-split bonding and antibonding states nearby the Fermi level. Furthermore, the inversion of the GGA + U V magnetic moment can be described by a similar mechanism previously observed for Fe/BTO [20]. The switch of polarization from P_{down} to P_{up} increases the overlap between the V and Ti states causing the minority-spin d_{xz} states of V to move below the Fermi energy, whereas the majority-spin states shift towards the Fermi level to preserve charge neutrality. Hence, the reversal causes the concurrent population of the minority- and depopulation of the majority-spin states, which is the major contribution for the interfacial ME effect observed at the V-rich interface. Notice that GGA predicts a much weaker coupling because the d states of V are not so exchange split and the increase of hybridization occurs in both majority and minority channels. The addition of Hubbard correction increases the localization of the electrons in both Ti

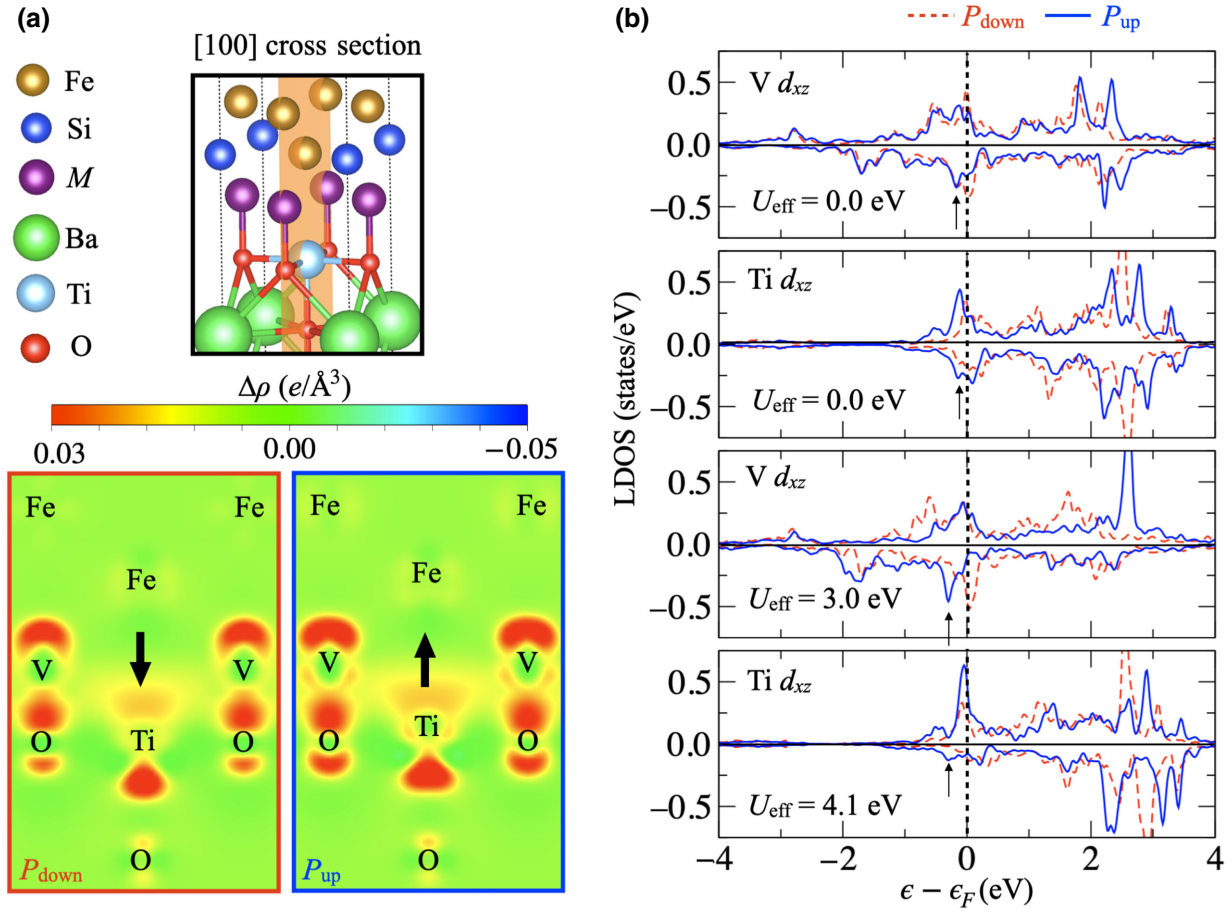

FIG. 6. PBEsol results for (a) the electron density difference, $\Delta\rho$, upon the $Fe_3Si/V/BaTiO_3$ formation from the FM and FE phases frozen in their interface relaxed configurations. (b) The local density of states for the d_{xz} V and d_{xz} Ti states in the heterostructure. The dashed red and solid blue lines correspond to the P_{down} and P_{up} configurations, respectively. The dashed vertical line indicates the Fermi energy, which is located at 0.00 eV.

and M and amplifies the exchange split of the M d states, generally leading to larger magnetoelectricity. However, in some cases such as the Cr the coupling is hindered because the shift of the d states decreases the DOS nearby the Fermi level, as shown in Figs. S9 and S10 within the Supplemental Material [39].

Although we identify the mechanism of coupling as being driven by interface hybridization, we still need to address the ME effect trends shown in Fig. 3 and the reasons leading to the strong coupling at the V- and Mn-rich interfaces. As previous studies have shown [20–22], bonding-driven coupling depends on the formation of exchange-split bonding and antibonding states and for that two conditions are required: (i) the d states of the interface M atoms should be exchange split; and (ii) these states should overlap strongly with Ti d states. Based on our results, we add a third requirement: (iii) the polarization reversal should change considerably the interface structure of the heterostructure to change the M—Ti bond length. In our systems, for the second condition to be met, the metal should have a large DOS around 2 eV above the Fermi level. From the LDOS for the isolated monolayers, shown in the Supplemental Material [39], it can be seen that the late metals (Ni, Cu, and Zn groups) fail to meet this condition. The interface structure is pinned for the junctions rich in early TMs due to the M—Ti Coulombic repulsion. The magnetoelectricity is hard to build for the interfaces containing 4d metals because their electronic states present less exchange splitting and the d bands are comparatively wider than their 3d counterparts, leading to a low DOS around the Fermi level. Naturally, all the interfaces with noticeable ME coupling meet the three conditions for hybridization. At least for the GGA calculations, the remarkable ME effect found for the Cr and Mn systems seems to be related with the near unoccupancy of one of the spin-channel d band, which is pushed to higher energies above the Fermi level, where the overlap with Ti d states is stronger. Because both metals present a formal d^5 electron configuration prior to the interface formation, the exchange-split interfacial bonding and ME coupling

might be enhanced if this "d^5-ness" feature is achieved in the interface metallic layer.

H. Feasibility of the V- and Mn-rich interfaces

Among the studied heterojunctions, the V- and Mn-rich interfaces emerge as the most promising systems for spintronic devices due to the strong correlation between the interface magnetic properties and the polarization of the FE phase. To estimate the amount of ME coupling in these systems, we adopt a widely used [20–23] figure of merit for multiferroics known as the interface ME coefficient, α_{int}, which is defined as

$$\alpha_{\text{int}} = \frac{\mu_0 \Delta m_{\text{int}}}{EA}, \tag{2}$$

where μ_0 is the vacuum permeability and E is the electric field used to reverse the FE polarization, which is assumed to be equivalent to the coercive field of $BaTiO_3$ ($E = E_c = 10^5$ V m^{-1}). Thus, in contrast to the ME effect observed in the surface of some ferromagnets [23], the coupling here is nonlinear due to the hysteretic dependence of BTO polarization on the electric field. For the V- and Mn-rich interfaces, we calculate the PBEsol ME coefficients to be 9.3×10^{-19} s and 1.3×10^{-18} s, respectively. Depending on the value of U_{eff} applied, the coefficients increase to up to 8.6×10^{-18} s (V) and 2.8×10^{-18} s (Mn). These represent an enhancement of up to 12 and 4 times on the ME coupling found at the ordinary $Fe_3Si/BaTiO_3$ interface ($\alpha_{\text{int}} = 0.49 \times 10^{-19} \sim 7.0 \times 10^{-19}$ s). For example, the largest estimation of ME coefficient for the V-rich interfaces is larger by a factor of 4 when compared to reported heterostructures like $Fe/BaTiO_3$ (2.2×10^{-18} s) [20], and $Fe_3O_4/BaTiO_3$ (2.1×10^{-18} s) [21].

In principle, the results of interfacial separation work indicates that the V- and Mn-rich interfaces are among the systems with a large interface bonding strength. Naturally, a proper assessment of the interface stability should take into account temperature effects through, for example, molecular dynamics coupled with reactive force fields, which is beyond the scope of this study. Nevertheless, we could still provide an approximate estimation of the interface stability against the replacement of the M atoms by nearby atoms. Therefore, we calculate the energy change when the M atoms are replaced by the nearest Fe, Si, or both atoms, E_{sub}, which is more likely to occur when compared to O and Ti atoms owing to their strong binding to the oxide phase. The results for both polarizations are summarized in Table II. The Mn-rich interface is found to be stable against the interchange with the atoms from the FM phase as the replacement energy penalty varies from 0.25 to 0.58 eV. Our results indicate that the V atoms should not be replaced by Si, however, the interchange with nearby Fe atoms is energetically favorable. A simultaneous replacement by the Fe and Si atoms leads to a configuration slightly more stable but the polarization reversal from P_{down} to P_{up} seems to invert the trend because Si atoms cannot interact with the t_{2g} orbitals of the protruding Ti as strong as the V atom can. Thus, based on the magnitude of E_{sub}, we would expect the VFe composition in the P_{up} rather than FeSi, yet one should not discard the possibility of a metastable V-rich interface at room temperature.

TABLE II. The PBEsol energy change (in eV) per supercell upon the interchange of M atoms by the nearest Fe, Si, and FeSi, namely, $E_{\text{sub}}^{\text{Fe}}$, $E_{\text{sub}}^{\text{Si}}$, and $E_{\text{sub}}^{\text{FeSi}}$, respectively. The values are given for both polarizations.

	P_{down}			P_{up}		
System	$E_{\text{sub}}^{\text{Fe}}$	$E_{\text{sub}}^{\text{Si}}$	$E_{\text{sub}}^{\text{FeSi}}$	$E_{\text{sub}}^{\text{Fe}}$	$E_{\text{sub}}^{\text{Si}}$	$E_{\text{sub}}^{\text{FeSi}}$
V	−0.21	0.18	−0.03	−0.23	0.21	0.02
Mn	0.26	0.50	0.38	0.25	0.58	0.48

Finally, we suggest that our heterostructures could be produced by an initial atomic layer deposition of the M monolayer on $BaTiO_3(001)$ followed by the epitaxial growth of Fe_3Si, which should be facilitated due to the small lattice mismatch between the FE and FM phases. Although we acknowledge that the deposition of V or Mn films on BTO is not a trivial task, especially due to possible oxidation of the metal monolayer, the growth of high-quality films on several substrates could be achieved due to the continuous advancement of atomic deposition techniques [67,68].

IV. CONCLUSION

We investigate via DFT the magnetoelectric effect at the interface of ferroelectric/ferromagnetic $Fe_3Si/M/BaTiO_3$ (001) heterostructures, where M represented $3d$ (Sc to Zn) and $4d$ (Y to Cd) metals. Our methodology addresses common deficiencies of GGA functionals such as the volume overestimation and the underestimation of the band gap, which could lead to an incorrect description of the interface interactions. Our discussion is supported by a set of structural, energetic, and electronic properties obtained, which reaches beyond the audience of multiferroics, and can also be of interest to the general communities of metal-semiconductor junctions and interface science.

The overestimation of lattice parameters leads to the overpolarization of the ferroelectric phase and, consequently, to the prediction of larger magnetoelectricity at the interfaces. The use of PBEsol reduces significantly the overestimation of the ferroelectric polarization, resulting in the computation of significantly smaller changes of magnetization due to the reversal of the polarization direction. In general, the addition of Hubbard-U correction predicts a stronger multiferroicity, which is very dependent on the value of U_{eff}. The on-site Coulomb corrections increase the

exchange split and localization of the metal d states. In some systems, such as for the Cr-rich interface, it decreases the ME effect by shifting states off the region nearby the Fermi level. Nevertheless, the GGA + U followed the general trends of the plain GGA calculations. Our results predict that the magnetoelectricity of the Fe_3Si/BTO can be enhanced by up to 12 and 4 times by replacing the interface Fe atoms with V and Mn, respectively.

The ME effect at the present systems is driven by bond effects at the interface. Based on present and previous results [20–22], three conditions are necessary to induce bonding-driven multiferroicity: (i) the d states of the interface M atoms should be exchange split; (ii) should overlap strongly with Ti d states to generate exchange-split bonding and antibonding states; (iii) the reversal of the polarization should effectively modify the interface structure to change the M—Ti bond length. The overall tendencies for the $Fe_3Si/M/BaTiO_3$ interfaces suggest that a formal d^5 electron configuration for the interface M pushes the minority-spin d states to higher-energy levels, which strengthens the bonding with the interface Ti atoms. Hence, the "d^5-ness" condition of the interface atoms, characterized by the near emptiness of one of the d spin channels, should increase the expected ME coupling. This result expands on the previous conception [20] that the hybridization between transition metals with less than half occupied d bands (like Ti) and more than half occupied d bands (like Fe) is the primary cause of magnetoelectricity.

ACKNOWLEDGMENTS

This work is financed in part by CREST-JST (Grant No. JPMJCR18J1), Program for Promoting Researches on the Supercomputer Fugaku, DPMSD by MEXT, JSPS-KAKENHI (Grant No. 17K04978), and CSRN in Osaka University. The calculations are partly carried out by using HPC resources at the Institute for Solid State Physics (ISSP), The University of Tokyo, and TSUBAME, Tokyo Institute of Technology.

[1] M. M. Waldrop, The chips are down for Moore's law, Nature **530**, 144 (2016).
[2] P. Chandra, M. Dawber, P. B. Littlewood, and J. F. Scott, Scaling of the coercive field with thickness in thin-film ferroelectrics, Ferroelectrics **313**, 7 (2004).
[3] S. Manipatruni, D. E. Nikonov, and I. A. Young, Beyond CMOS computing with spin and polarization, Nat. Phys. **14**, 338 (2018).
[4] N. A. Spaldin and R. Ramesh, Advances in magnetoelectric multiferroics, Nat. Mater. **18**, 203 (2019).
[5] T. Taniyama, Electric-field control of magnetism via strain transfer across ferromagnetic/ferroelectric interfaces, J. Phys.: Condens. Matter **27**, 504001 (2015).
[6] N. A. Hill, Why are there so few magnetic ferroelectrics?, J. Phys. Chem. B **104**, 6694 (2000).
[7] C. A. F. Vaz, J. Hoffman, C. H. Ahn, and R. Ramesh, Magnetoelectric coupling effects in multiferroic complex oxide composite structures, Adv. Mater. **22**, 2900 (2010).
[8] W. Eerenstein, M. Wiora, J. L. Prieto, J. F. Scott, and N. D. Mathur, Giant sharp and persistent converse magnetoelectric effects in multiferroic epitaxial heterostructures, Nat. Mater. **6**, 348 (2007).
[9] H. F. Tian, T. L. Qu, L. B. Luo, J. J. Yang, S. M. Guo, H. Y. Zhang, Y. G. Zhao, and J. Q. Li, Strain induced magnetoelectric coupling between magnetite and $BaTiO_3$, Appl. Phys. Lett. **92**, 063507 (2008).
[10] M. Staruch, J. F. Li, Y. Wang, D. Viehland, and P. Finkel, Giant magnetoelectric effect in nonlinear Metglas/PIN-PMN-PT multiferroic heterostructure, Appl. Phys. Lett. **105**, 152902 (2014).
[11] Y. Shirahata, R. Shiina, D. L. González, K. J. A. Franke, E. Wada, M. Itoh, N. A. Pertsev, S. van Dijken, and T. Taniyama, Electric-field switching of perpendicularly magnetized multilayers, NPG Asia Mater. **7**, e198 (2015).
[12] A. Swain, K. Komatsu, M. Itoh, T. Taniyama, and V. Gorige, Strain-mediated magnetic response in $La_{0.67}Sr_{0.33}MnO_3/SrTiO_3/La_{0.67}Sr_{0.33}MnO_3/BaTiO_3$ structure, AIP Adv. **8**, 055808 (2017).
[13] V. Skumryev, V. Laukhin, I. Fina, X. Martí, F. Sánchez, M. Gospodinov, and J. Fontcuberta, Magnetization Reversal by Electric-Field Decoupling of Magnetic and Ferroelectric Domain Walls in Multiferroic-Based Heterostructures, Phys. Rev. Lett. **106**, 057206 (2011).
[14] J. T. Heron, M. Trassin, K. Ashraf, M. Gajek, Q. He, S. Y. Yang, D. E. Nikonov, Y.-H. Chu, S. Salahuddin, and R. Ramesh, Electric-Field-Induced Magnetization Reversal in a Ferromagnet-Multiferroic Heterostructure, Phys. Rev. Lett. **107**, 217202 (2011).
[15] J. T. Heron, D. G. Schlom, and R. Ramesh, Electric field control of magnetism using $BiFeO_3$-based heterostructures, Appl. Phys. Rev. **1**, 021303 (2014).
[16] J. T. Heron, J. L. Bosse, Q. He, Y. Gao, M. Trassin, L. Ye, J. D. Clarkson, C. Wang, J. Liu, S. Salahuddin, D. C. Ralph, D. G. Schlom, J. Íñiguez, B. D. Huey, and R. Ramesh, Deterministic switching of ferromagnetism at room temperature using an electric field, Nature **516**, 370 (2014).
[17] K. Fujita and Y. Gohda, First-Principles Study of Magnetoelectric Coupling at $Fe/BiFeO_3(001)$ Interfaces, Phys. Rev. Appl. **11**, 024006 (2019).
[18] J. M. Rondinelli, M. Stengel, and N. A. Spaldin, Carrier-mediated magnetoelectricity in complex oxide heterostructures, Nat. Nanotechnol. **3**, 46 (2007).
[19] H. J. A. Molegraaf, J. Hoffman, C. A. F. Vaz, S. Gariglio, D. van der Marel, C. H. Ahn, and J.-M. Triscone, Magnetoelectric effects in complex oxides with competing ground states, Adv. Mater. **21**, 3470 (2009).
[20] C.-G. Duan, S. S. Jaswal, and E. Y. Tsymbal, Predicted Magnetoelectric Effect in $Fe/BaTiO_3$ Multilayers: Ferroelectric Control of Magnetism, Phys. Rev. Lett. **97**, 047201 (2006).
[21] M. K. Niranjan, J. P. Velev, C.-G. Duan, S. S. Jaswal, and E. Y. Tsymbal, Magnetoelectric effect at the $Fe_3O_4/BaTiO_3(001)$ interface: A first-principles study, Phys. Rev. B **78**, 104405 (2008).

[22] Y. Hamazaki and Y. Gohda, Enhancement of magnetoelectric coupling by insertion of Co atomic layer into $Fe_3Si/BaTiO_3(001)$ interfaces identified by first-principles calculations, J. Appl. Phys. **126**, 233902 (2019).

[23] C.-G. Duan, J. P. Velev, R. F. Sabirianov, Z. Zhu, J. Chu, S. S. Jaswal, and E. Y. Tsymbal, Surface Magnetoelectric Effect in Ferromagnetic Metal Films, Phys. Rev. Lett. **101**, 137201 (2008).

[24] V. Corral-Flores, D. Bueno-Baqués, and R. Ziolo, Synthesis and characterization of novel $CoFe_2O_4 - BaTiO_3$ multiferroic core–shell-type nanostructures, Acta Mater. **58**, 764 (2010).

[25] Z. Wang, J. Hu, and M.-F. Yu, Axial polarization switching in ferroelectric $BaTiO_3$ nanowire, Nanotechnol. **18**, 235203 (2007).

[26] R. Le Dantec, Y. Mugnier, G. Djanta, L. Bonacina, J. Extermann, L. Badie, C. Joulaud, M. Gerrmann, D. Rytz, J. P. Wolf, and C. Galez, Ensemble and individual characterization of the nonlinear optical properties of ZnO and $BaTiO_3$ nanocrystals, J. Phys. Chem. C **115**, 15140 (2011).

[27] C.-F. Chen, G. King, R. M. Dickerson, P. A. Papin, S. Gupta, W. R. Kellogg, and G. Wu, Oxygen-deficient $BaTiO_{3-x}$ perovskite as an efficient bifunctional oxygen electrocatalyst, Nano Energy **13**, 423 (2015).

[28] Y. Nakamura, *Alloys and Compounds of d-Elements with Main Group Elements. Part 2*, (Landolt-Börnstein, New Series, Group III; Springer Verlag: Berlin, 1988), Vol. 19, p. 26.

[29] R. Wahl, D. Vogtenhuber, and G. Kresse, $SrTiO_3$ and $BaTiO_3$ revisited using the projector augmented wave method: Performance of hybrid and semilocal functionals, Phys. Rev. B **78**, 104116 (2008).

[30] J. P. Perdew, K. Burke, and M. Ernzerhof, Generalized Gradient Approximation Made Simple, Phys. Rev. Lett. **77**, 3865 (1996).

[31] M. Stengel, P. Aguado-Puente, N. A. Spaldin, and J. Junquera, Band alignment at metal/ferroelectric interfaces: Insights and artifacts from first principles, Phys. Rev. B **83**, 235112 (2011).

[32] D. Di Sante, K. Yamauchi, and S. Picozzi, Beyond standard local density approximation in the study of magnetoelectric effects in $Fe/BaTiO_3$ and $Co/BaTiO_3$ interfaces, J. Phys.: Condens. Matter **25**, 066001 (2013).

[33] J. P. Perdew, A. Ruzsinszky, G. I. Csonka, O. A. Vydrov, G. E. Scuseria, L. A. Constantin, X. Zhou, and K. Burke, Restoring the Density-Gradient Expansion for Exchange in Solids and Surfaces, Phys. Rev. Lett. **100**, 136406 (2008).

[34] S. L. Dudarev, G. A. Botton, S. Y. Savrasov, C. J. Humphreys, and A. P. Sutton, Electron-energy-loss spectra and the structural stability of nickel oxide: An LSDA+U study, Phys. Rev. B **57**, 1505 (1998).

[35] P. E. Blöchl, Projector augmented-wave method, Phys. Rev. B **50**, 17953 (1994).

[36] G. Kresse and J. Hafner, *Ab initio* molecular dynamics for open-shell transition metals, Phys. Rev. B **48**, 13115 (1993).

[37] G. Kresse and J. Furthmüller, Efficient iterative schemes for *ab initio* total-energy calculations using a plane-wave basis set, Phys. Rev. B **54**, 11169 (1996).

[38] G. Kresse and D. Joubert, From ultrasoft pseudopotentials to the projector agumented-wave method, Phys. Rev. B **59**, 1758 (1999).

[39] See Supplemental Material at http://link.aps.org/supplemental/10.1103/PhysRevApplied.15.064014 for details on the PAW potentials, properties of bulk phase, extra results of energetic, structural, and electronic properties of the heterostructures, and density of states of the isolated monolayers and magnetic phase.

[40] M. Cococcioni and S. de Gironcoli, Linear response approach to the calculation of the effective interaction parameters in the LDA+U method, Phys. Rev. B **71**, 035105 (2005).

[41] G. H. Kwei, A. C. Lawson, S. J. L. Billinge, and S. W. Cheong, Structures of the ferroelectric phases of barium titanate, J. Phys. Chem. **97**, 2368 (1993).

[42] H. H. Wieder, Electrical behavior of barium titanate single crystals at low temperatures, Phys. Rev. **99**, 1161 (1955).

[43] J. Lee, N. Sai, T. Cai, Q. Niu, and A. A. Demkov, Interfacial magnetoelectric coupling in tricomponent superlattices, Phys. Rev. B **81**, 144425 (2010).

[44] B. D. Begg, E. R. Vance, and J. Nowotny, Effect of particle size on the room-temperature crystal structure of barium titanate, J. Am. Ceram. Soc. **77**, 3186 (1994).

[45] F. Tsai and J. M. Cowley, Thickness dependence of ferroelectric domains in thin crystalline films, Appl. Phys. Lett. **65**, 1906 (1994).

[46] S. Dennler and J. Hafner, First-principles study of lattice dynamics and diffusion in DO_3-type Fe_3Si, Phys. Rev. B **73**, 174303 (2006).

[47] O. G. Randl, G. Vogl, W. Petry, B. Hennion, B. Sepiol, and K. Nembach, Lattice dynamics and related diffusion properties of intermetallics: I. Fe_3Si, J. Phys.: Condens. Matter **7**, 5983 (1995).

[48] W. A. Hines, A. H. Menotti, J. I. Budnick, T. J. Burch, T. Litrenta, V. Niculescu, and K. Raj, Magnetization studies of binary and ternary alloys based on Fe_3Si, Phys. Rev. B **13**, 4060 (1976).

[49] A. Paoletti and L. Passari, A polarized neutron investigation of the Fe_3Si alloy, Nuovo Cim. **32**, 25 (1964).

[50] I. I. Oleinik, E. Y. Tsymbal, and D. G. Pettifor, Atomic and electronic structure of $Co/SrTiO_3/Co$ magnetic tunnel junctions, Phys. Rev. B **65**, 020401(R) (2001).

[51] W. A. Saidi, Trends in the adsorption and growth morphology of metals on the $MoS_2(001)$ surface, Cryst. Growth Des. **15**, 3190 (2015).

[52] R. Costa-Amaral, A. Forhat, N. A. Caturello, and J. L. F. Da Silva, Unveiling the adsorption properties of 3*d*, 4*d*, and 5*d* metal adatoms on the MoS_2 monolayer: A DFT-D3 investigation, Surf. Sci. **701**, 121700 (2020).

[53] H. Valencia, A. Gil, and G. Frapper, Trends in the adsorption of 3*d* transition metal atoms onto graphene and nanotube surfaces: A DFT study and molecular orbital analysis, J. Phys. Chem. C **114**, 14141 (2010).

[54] R. Costa-Amaral and Y. Gohda, First-principles study of the adsorption of 3*d* transition metals on BaO- and TiO_2-terminated cubic-phase $BaTiO_3(001)$ surfaces, J. Chem. Phys. **152**, 204701 (2020).

[55] J. C. Slater, Atomic radii in crystals, J. Chem. Phys. **41**, 3199 (1964).

[56] Y. Zhao, J.-J. Zhang, S. Yuan, and Z. Chen, Nonvolatile electrical control and heterointerface-induced half-metallicity of 2D ferromagnets, Adv. Funct. Mater. **29**, 1901420 (2019).
[57] G. Henkelman, A. Arnaldsson, and H. Jónsson, A fast and robust algorithm for bader decomposition of charge density, Comput. Mater. Sci. **36**, 354 (2006).
[58] W. Zhong, R. D. King-Smith, and D. Vanderbilt, Giant LO-TO Splittings in Perovskite Ferroelectrics, Phys. Rev. Lett. **72**, 3618 (1994).
[59] N. F. Mott, The theory of crystal rectifiers, Proc. R. Soc. London, Ser. A **171**, 27 (1939).
[60] R. T. Tung, The physics and chemistry of the schottky barrier height, Appl. Phys. Rev. **1**, 011304 (2014).
[61] V. Heine, Theory of surface states, Phys. Rev. **138**, A1689 (1965).
[62] F. Rao, M. Kim, A. J. Freeman, S. Tang, and M. Anthony, Structural and electronic properties of transition-metal/$BaTiO_3$(001) interfaces, Phys. Rev. B **55**, 13953 (1997).
[63] J. Bardeen, Surface states and rectification at a metal semiconductor contact, Phys. Rev. **71**, 717 (1947).
[64] C. Berthod, N. Binggeli, and A. Baldereschi, Local interface dipoles and the tuning of the Al/GaAs(100) schottky-barrier height with ultrathin Si interlayers, Europhys. Lett. **36**, 67 (1996).
[65] S. Tanaka, T. Tamura, K. Okazaki, S. Ishibashi, and M. Kohyama, Schottky-barrier heights of metal/alpha-SiC{0001} interfaces by first-principles calculations, Phys. Status Solidi C **4**, 2972 (2007).
[66] J. Mucelini, R. Costa-Amaral, Y. Seminovski, and J. L. F. Da Silva, Ab initio investigation of the formation of ZrO_2-like structures upon the adsorption of Zr_n on the CeO_2(111) surface, J. Chem. Phys. **149**, 244702 (2018).
[67] B. S. Lim, A. Rahtu, and R. G. Gordon, Atomic layer deposition of transition metals, Nat. Mater. **2**, 749 (2003).
[68] R. W. Johnson, A. Hultqvist, and S. F. Bent, A brief review of atomic layer deposition: From fundamentals to applications, Mater. Today **17**, 236 (2014).